Optical manipulation of self-aligned graphene flakes in liquid crystals

Christopher W. Twombly,[1] Julian S. Evans,[1] and Ivan I. Smalyukh[1,2,3,*]

[1]*Department of Physics and Liquid Crystal Materials Research Center, University of Colorado, Boulder, Colorado 80309, USA*

[2]*Department of Electrical, Computer, and Energy Engineering and Materials Science Engineering Program, University of Colorado, Boulder, Colorado 80309, USA*

[3]*Renewable and Sustainable Energy Institute, National Renewable Energy Laboratory and University of Colorado, Boulder, Colorado 80309, USA*

[*] *ivan.smalyukh@colorado.edu*

Abstract: Graphene recently emerged as a new two-dimensional material platform with unique optical, thermal and electronic properties. Single- or few-atom-thick graphene flakes can potentially be utilized to form structured bulk composites that further enrich these properties and enable a broad range of new applications. Here we describe optical manipulation of self-aligned colloidal graphene flakes in thermotropic liquid crystals of nematic and cholesteric types. Three-dimensional rotational and translational manipulation of graphene flakes by means of holographic optical tweezers allows for non-contact spatial patterning of graphene, control of liquid crystal defects, and low-power optical realignment of the liquid crystal director using these flakes. Potential applications include optically- and electrically-controlled reconfigurable liquid crystalline dispersions of spontaneously aligning colloidal graphene flakes and new electro-optic devices with graphene-based interconnected transparent electrodes at surfaces and in the bulk of liquid crystals.

OCIS codes: (160.3710) Liquid crystals; (140.7010) Laser trapping; (160.4236) Nanomaterials; (180.6900) Three-dimensional microscopy.

References and links

1. P. Poulin, H. Stark, T. C. Lubensky, and D. A. Weitz, "Novel colloidal interactions in anisotropic fluids," Science **275**(5307), 1770–1773 (1997).
2. P. Poulin and D. A. Weitz, "Inverted and multiple nematic emulsions," Phys. Rev. E Stat. Phys. Plasmas Fluids Relat. Interdiscip. Topics **57**(1), 626–637 (1998).
3. A. Martinez, H. C. Mireles, and I. I. Smalyukh, "Large-area optoelastic manipulation of colloidal particles in liquid crystals using photoresponsive molecular surface monolayers," Proc. Natl. Acad. Sci. U.S.A. **108**(52), 20891–20896 (2011).
4. Y. Gu and N. L. Abbott, "Observation of saturn-ring defects around solid microspheres in nematic liquid crystals," Phys. Rev. Lett. **85**(22), 4719–4722 (2000).
5. S. J. Woltman, G. D. Jay, and G. P. Crawford, "Liquid-crystal materials find a new order in biomedical applications," Nat. Mater. **6**(12), 929–938 (2007).
6. C. P. Lapointe, T. G. Mason, and I. I. Smalyukh, "Shape-controlled colloidal interactions in nematic liquid crystals," Science **326**(5956), 1083–1086 (2009).
7. J. S. Evans, C. Beier, and I. I. Smalyukh, "Alignment of high-aspect ratio colloidal gold nanoplatelets in nematic liquid crsytals," J. Appl. Phys. **110**(3), 033535 (2011).
8. T. Yamamoto, Y. Tabe, and H. Yokoyama, "Manipulation of defect structures and colloidal chains in liquid crystals by means of photochemical reactions of azobenzene compounds," Colloids Surf. A Physicochem. Eng. Asp. **334**, 155–159 (2009).
9. Q. Liu, Y. Cui, D. Gardner, X. Li, S. He, and I. I. Smalyukh, "Self-alignment of plasmonic gold nanorods in reconfigurable anisotropic fluids for tunable bulk metamaterial applications," Nano Lett. **10**(4), 1347–1353 (2010).
10. G. M. Koenig, Jr., I.-H. Lin, and N. L. Abbott, "Chemoresponsive assemblies of microparticles at liquid crystalline interfaces," Proc. Natl. Acad. Sci. U.S.A. **107**(9), 3998–4003 (2010).

#179756 - $15.00 USD Received 12 Nov 2012; revised 24 Dec 2012; accepted 24 Dec 2012; published 11 Jan 2013

11. M. R. Jones, R. J. Macfarlane, B. Lee, J. Zhang, K. L. Young, A. J. Senesi, and C. A. Mirkin, "DNA-nanoparticle superlattices formed from anisotropic building blocks," Nat. Mater. **9**(11), 913–917 (2010).
12. P. M. Chaikin and T. C. Lubensky, *Principles of Condensed Matter Physics* (Cambridge University Press, 1995).
13. M. Zapotocky, L. Ramos, P. Poulin, T. C. Lubensky, and D. A. Weitz, "Particle-stabilized defect gel in cholesteric liquid crystals," Science **283**(5399), 209–212 (1999).
14. M. Ravnik, G. P. Alexander, J. M. Yeomans, and S. P. Žumer, "Three-dimensional colloidal crystals in liquid crystalline blue phases," Proc. Natl. Acad. Sci. U.S.A. **108**(13), 5188–5192 (2011).
15. D. Engström, R. P. Trivedi, M. Persson, K. A. Bertness, M. Goksör, and I. I. Smalyukh, "Three-dimensional imaging of liquid crystal structures and defects by means of holographic manipulation of colloidal nanowires with faceted sidewalls," Soft Matter **7**(13), 6304–6312 (2011).
16. R. P. Trivedi, D. Engström, and I. I. Smalyukh, "Optical manipulation of colloids and defect structures in anisotropic liquid crystal fluids," J. Opt. **13**(4), 044001 (2011).
17. B. Senyuk, J. S. Evans, P. Ackerman, T. Lee, P. Manna, L. Vigderman, E. R. Zubarev, J. van de Lagemaat, and I. I. Smalyukh, "Shape-dependent oriented trapping and scaffolding of plasmonic nanoparticles by topological defects for self-assembly of colloidal dimers in liquid crystals," Nano Lett. **12**(2), 955–963 (2012).
18. A. Martinez, T. Lee, T. Asavei, H. Rubinsztein-Dunlop, and I. I. Smalyukh, "Three-dimensional complex-shaped photopolymerized microparticles at liquid crystal interfaces," Soft Matter **8**(8), 2432–2437 (2012).
19. K. S. Novoselov, A. K. Geim, S. V. Morozov, D. Jiang, Y. Zhang, S. V. Dubonos, I. V. Grigorieva, and A. A. Firsov, "Electric field effect in atomically thin carbon films," Science **306**(5696), 666–669 (2004).
20. O. M. Maragó, F. Bonaccorso, R. Saija, G. Privitera, P. G. Gucciardi, M. A. Iatì, G. Calogero, P. H. Jones, F. Borghese, P. Denti, V. Nicolosi, and A. C. Ferrari, "Brownian motion of graphene," ACS Nano **4**(12), 7515–7523 (2010).
21. D. W. Kim, Y. H. Kim, H. S. Jeong, and H.-T. Jung, "Direct visualization of large-area graphene domains and boundaries by optical birefringency," Nat. Nanotechnol. **7**, 29–34 (2012).
22. X. Wang, Y. P. Chen, and D. D. Nolte, "Strong anomalous optical dispersion of graphene: complex refractive index measured by Picometrology," Opt. Express **16**(26), 22105–22112 (2008).
23. J. M. Dawlaty, S. Shivaraman, J. Strait, P. George, M. Chandrashekhar, F. Rana, M. G. Spencer, D. Veksler, and Y. Chen, "Broadband electromagnetic response and ultrafast dynamics of few-layer epitaxial graphene," Appl. Phys. Lett. **94**, 172102 (2009).
24. R. P. Trivedi, I. I. Klevets, B. I. Senyuk, T. Lee, and I. I. Smalyukh, "Reconfigurable interactions and three-dimensional patterning of colloidal particles and defects in lamellar soft media," Proc. Natl. Acad. Sci. U.S.A. **109**(13), 4744–4749 (2012).
25. A. I. Bishop, T. A. Nieminen, N. R. Heckenberg, and H. Rubinsztein-Dunlop, "Measurement of the total optical angular momentum transfer in optical tweezers," Opt Express **14**, 6963 (2006).
26. Y. Yang, P. D. Brimicombe, N. W. Roberts, M. R. Dickinson, M. Osipov, and H. F. Gleeson, "Continuously rotating chiral liquid crystal droplets in a linearly polarized laser trap," Opt. Express **16**(10), 6877–6882 (2008).
27. P. Galajda and P. Ormos, "Complex micromachines produced and driven by light," Appl. Phys. Lett. **78**(2), 249–251 (2001).
28. K. D. Bonin, B. Kourmanov, and T. G. Walker, "Light torque nanocontrol, nanomotors and nanorockers," Opt. Express **10**(19), 984–989 (2002).
29. P. H. Jones, F. Palmisano, F. Bonaccorso, P. G. Gucciardi, G. Calogero, A. C. Ferrari, and O. M. Maragó, "Rotation detection in light-driven nanorotors," ACS Nano **3**(10), 3077–3084 (2009).
30. S. H. Simpson, D. C. Benito, and S. Hanna, "Polarization-induced torque in optical traps," Phys. Rev. A **76**(4), 043408 (2007).
31. B. Senyuk, Q. Liu, S. He, R. D. Kamien, R.B. Kusner, T. C. Lubensky, and I. I. Smalyukh. "Topological colloids." doi:10.1038/nature11710 (2012).
32. S. Stankovich, D. A. Dikin, G. H. B. Dommett, K. M. Kohlhaas, E. J. Zimney, E. A. Stach, R. D. Piner, S. T. Nguyen, and R. S. Ruoff, "Graphene-based composite materials," Nature **442**(7100), 282–286 (2006).
33. P. Blake, P. D. Brimicombe, R. R. Nair, T. J. Booth, D. Jiang, F. Schedin, L. A. Ponomarenko, S. V. Morozov, H. F. Gleeson, E. W. Hill, A. K. Geim, and K. S. Novoselov, "Graphene-based liquid crystal device," Nano Lett. **8**(6), 1704–1708 (2008).
34. F. Bonaccorso, Z. Sun, T. Hasan, and A. C. Ferrari, "Graphene photonics and optoelectronics," Nat. Photonics **4**(9), 611–622 (2010).
35. Q. Liu, T. Asavei, T. Lee, H. Rubinsztein-Dunlop, S. He, and I. I. Smalyukh, "Measurement of viscosity of lyotropic liquid crystals by means of rotating laser-trapped microparticles," Opt. Express **19**(25), 25134–25143 (2011).

1. Introduction

Liquid crystals (LCs) can serve as optically- and electrically-reconfigurable fluid hosts for spontaneous alignment and assembly of dispersed colloidal particles into pre-designed configurations [1–10]. Particles locally alter the LC's molecular alignment and interact with the structured host fluid and with each other through surface anchoring and elastic forces that

#179756 - $15.00 USD Received 12 Nov 2012; revised 24 Dec 2012; accepted 24 Dec 2012; published 11 Jan 2013

are not encountered in conventional isotropic fluids and colloidal dispersions [11,12]. These interactions and the ensuing self-assembled and self-aligned structures can be further tailored by controlling the chirality of the host LC medium [13–15], the shape of the colloids [6,7,15,16], the boundary conditions for the director **n** (describing local average orientation of mesogenic molecules) at the LC-colloid interface [1,10], and the long-range patterns of molecular alignment **n**(**r**) in the surrounding LC. The latter can be switched by electric and magnetic fields, light, temperature, and mechanical stimuli, potentially enabling reconfigurable self-assembled colloidal structures. In addition to spherical colloids, LC-mediated interactions have been explored for particles with anisotropic shapes such as prolate and oblate polygonal prisms, discs, rods, and three-dimensional photopolymerized complex-shaped microparticles [1–10,13–18]. Even weak shape anisotropy of colloids typically results in their well-defined alignment in LCs [6,7,9,15–17]. Since both metallic and semiconductor nano- and microparticles can be used to form colloidal superstructures in LCs [1–10,13–17], they are of great interest for self-assembly of tunable materials with pre-designed structure, composition, anisotropic optical properties, and facile response to optical and electric fields.

In this work, we explore optical manipulation of dilute liquid crystalline dispersions of graphene flakes with aspect ratios ≥10,000, thickness comparable to the size of LC molecules, and lateral dimensions many orders of magnitude larger than their thickness. In nematic LCs, these random-shaped few-atoms-thick flakes tend to align parallel to the director **n** while freely rotating around **n**. In cholesteric LCs with pitch comparable to the flake size, flakes align parallel to **n** and perpendicular to the helical axis around which **n** twists. We use holographic optical tweezers (HOT), polarizing optical microscopy, and fluorescence confocal polarizing microscopy (FCPM) to probe the LC-mediated alignment of flakes as well as the structure of nematic and cholesteric LCs hosting them [16]. The facile response to focused laser beams and the well-defined alignment of graphene flakes in the LC allow for enhanced laser-induced realignment of **n**, non-contact optical manipulation, transfer of optical forces and torques, and may find applications in fabrication of graphene-based LC composites.

2. **Experimental techniques and sample preparation**

2.1 Materials

Graphene flakes were produced following the Geim-Novoselov method [19] by cleaving highly ordered pyrolytic graphite (purchased from Veeco) with scotch tape and then rubbing the tape with graphite on a glass surface. A suspension of graphite, freed graphene, and tape fragments in dichloromethane was produced by sonication of the glass substrate for one hour. The fragments of tape and graphite are removed from solution by two days of passive sedimentation. The top third of the suspension is transferred to a new vial and diluted to its original volume with dichloromethane. The sedimentation process is repeated twice to produce a suspension of few-atom-thick graphene flakes with lateral size of 2-20 μm. We then mix this suspension with 4-cyano-4'-pentylbiphenyl (5CB, purchased from Frinton Laboratories) or a cholesteric LC of pitch p ≈5 μm composed of a nematic host ZLI-2806 doped with a chiral agent CB15 at 3 wt. % (both obtained from EM Industries). This mixture is left at room temperature with no lid in a fume hood for 4 days so the dichloromethane fully evaporates, forming dilute nematic or cholesteric LC dispersions of well-separated graphene flakes at < 0.01 wt%. For FCPM studies, the LCs with graphene flakes are additionally doped with an anisotropic fluorescent dye n,n'-bis(2,5-di-tert-butylphenyl)-3,4,9,10-perylenedicarboximide (BTBP) at about 0.02 wt. % [15].

We have prepared both homeotropic and planar-aligned LC cells with graphene flakes. Glass plates were cleaned by sonication for 10 min each in acetone, isopropanol, and deionized water, followed by oxygen plasma cleaning. For homeotropic (perpendicular) surface alignment of **n**, the glass plates were dip-coated for 10 s in a 1 wt. % aqueous solution

#179756 - $15.00 USD Received 12 Nov 2012; revised 24 Dec 2012; accepted 24 Dec 2012; published 11 Jan 2013

of [3-(trimethoxysilyl)propyl]octadecyl-dimethylammonium chloride (DMOAP, purchased from Aldrich), rinsed with deionized water, and dried with compressed nitrogen gas. For planar alignment, a solution of 3 wt. % of polyimide PI-2555 in N-methyl-2-pyrrolidone (both obtained from HD Microsystems) was first filtered with a 10 μm particulate filter and spun coat onto the cleaned glass plates for 30 seconds at 400 rpm and, subsequently, for 1 min at 1500 rpm. The coated glass substrates were pre-baked at 110° C for 10 minutes to remove the solvent and then baked at 250° C for two hours to fully crosslink the polyimide. The substrates were subsequently rubbed with velvet cloth in a unidirectional fashion to set the direction of the easy axis for the planar LC alignment. The glass plates of both homeotropic and planar cells were spaced by ultraviolet-light-curable glue NOA-61 (from Norland) mixed with monodisperse glass spacers of diameter 10-60 μm to produce the desired cell gap. The cells were typically assembled from a thin glass plate of 170 μm thickness and a 1mm-thick glass plate in order to allow for imaging with the short working distance oil-immersion objectives. The cells were sealed with 5-min epoxy.

2.2 Optical setup for non-contact manipulation and imaging

We use a HOT setup integrated with an inverted optical microscope IX-81 and a confocal microscopy unit FV-300 (both from Olympus). All optical components are mounted on a vibration-isolated optical table (Newport) to provide high degree of stability. In the integrated imaging and manipulation setup, the same objective is used for optical trapping as well as imaging with both FCPM and conventional polarizing microscopy (PM). We use 60X and 100X Olympus oil immersion microscope objectives with numerical apertures NA ≈1.4 and ≈65% transmission at 1064nm. A dichroic mirror (Chroma) is mounted in a rotating filter turret positioned below an objective of the IX-81 microscope. The infrared trapping laser beam entering the microscope is reflected by the dichroic mirror into the objective lens while the visible light is transmitted to the charge-coupled device camera (Ptgrey, Flea 2, IEEE 1394b, up to 80 frames per second) and the confocal microscopy scanning head for both FCPM and PM imaging. The used BTBP dye is excited at 488nm and fluorescence emission is detected within 510-550 nm.

For optical manipulation, we employ a 1064 nm continuous wave, Ytterbium-doped fiber laser (YLM series, IPG Photonics, maximum power 10W) with a beam diameter of 5.0 μm. The beam is first expanded to overfill the active area of a spatial light modulator (SLM) and then reduced to the size of the back aperture of the objective. The trapping beam is linearly polarized using a Glan polarizer and its polarization direction is rotated using a half-wave retardation plate. Its phase is controlled on a pixel-by-pixel basis within 0-2π by a reflective, electrically addressed, phase-only, LC SLM (512 x 512 pixels with a pixel size of 15 x 15 μm^2, obtained from Boulder Nonlinear Systems) according to a holographic pattern supplied by a computer. The effective refresh rate of the SLM is 10-30 Hz for the entire array of pixels. The spatially modulated laser light is then imaged at the back aperture of the microscope objective acting as a Fourier transform lens. The holograms are generated using graphical software interface HOTkit (obtained from Arryx).

3. Results and discussion

3.1 Spontaneous alignment of graphene flakes in liquid crystals

The procedure of dispersing graphene flakes described above typically yields random-shaped single- or few-atom-thick graphene flakes with commonly observed folds (Fig. 1(a)). Since optical absorption is approximately linearly dependent (2.3% per layer [20]) on the number of atomic layers, we have optically selected flakes with thicknesses in the range from one to five layers. In nematic LCs, these flakes tend to spontaneously align parallel to the director **n** while being free to rotate around **n**, unless restricted by confinement into thin cells. By analyzing PM images, we concluded that flake edges do not perturb **n**(**r**) and have no direct

#179756 - $15.00 USD Received 12 Nov 2012; revised 24 Dec 2012; accepted 24 Dec 2012; published 11 Jan 2013

influence on orientation of the flake with respect to the far-field director $\mathbf{n_0}$, which is different from the case of much thicker lithographically generated colloidal platelets [6], but similar to about 5nm-thick polygonal gold platelets [7]. In cholesteric LCs with pitch p ≈5μm, comparable to the lateral flake size, we find flakes aligning parallel to the uniformly twisting director **n** and perpendicular to the helical axis **χ** (Figs. 1 and 2). FCPM and PM observations reveal that most of the flakes are suspended in the LC bulk for long periods of time (months) while undergoing Brownian motion (Figs. 1-3), although some flakes (~5%) sediment to surfaces.

The surface anchoring of the director **n** at graphene-LC interfaces is tangential due to pi-stacking [21] and not perturbed by flake edges, which is natural given that the thickness of graphene flakes is comparable or smaller than the LC molecular size. Therefore, a graphene flake of diameter D imposes an easy axis for the alignment of $\mathbf{n}(\mathbf{r})$ tangential to its surfaces. Using the Rapini-Papoular surface anchoring potential [12], one finds that the surface energy due to deviation of a small flake with D < 500nm for an angle θ from its equilibrium orientation parallel to $\mathbf{n_0}$ is $F_s = (\pi WD^2/4)\sin^2\theta$, where W is the polar surface anchoring coefficient. Using $W \approx 10^{-5}$ J/m^2 [21], one finds that $F_s >> k_BT$ even for flakes of D ~100nm barely observable in an optical microscope and at relatively small θ, explaining well defined self-alignment of the graphene flakes parallel to $\mathbf{n_0}$. As the flake size increases to D ≥ K/W ≈500 nm and larger, the alignment effects become even stronger and dominated by elasticity, where $K = (K_{11} + K_{22} + K_{33})/3$ is the average elastic constant (Table 1) and K_{11}, K_{22}, and K_{33} are splay, twist, and bend Frank elastic constants, respectively.

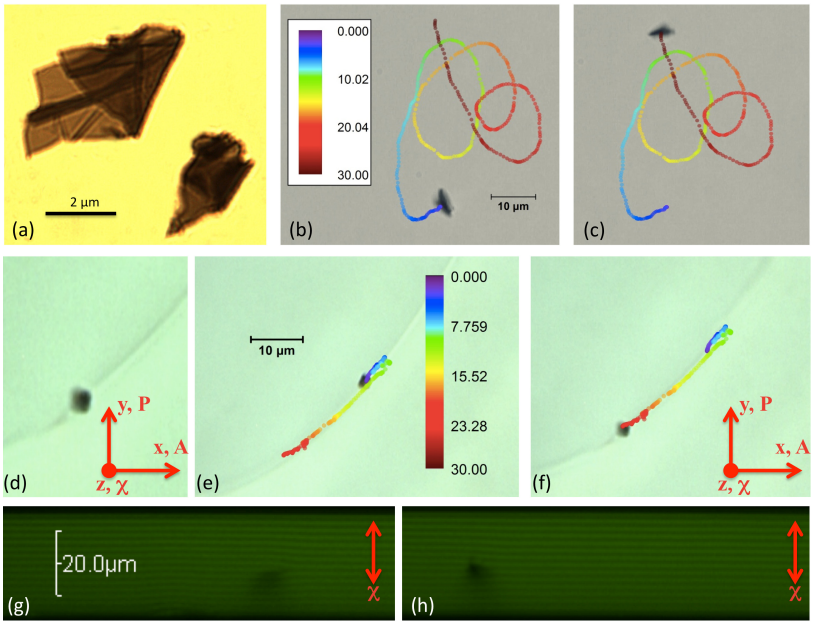

Fig. 1. Optical manipulation of graphene flakes in liquid crystals. (a) An optical micrograph of typical graphene flakes in immersion oil produced from cleaved highly ordered graphite; the folds and changes in layer thickness are visible as changes in optical transmission through the flakes. (b),(c) Computer-directed manipulation of an asymmetric graphene flake by laser tweezers in a cholesteric LC demonstrated by moving the flake along a time-coded trajectory with the flake shown in (b) initial and (c) final positions; the used laser power is 2.3 mW. (d-f) Optical micrographs showing (d) a graphene flake entrapped in a dislocation in a cholesteric LC that is optically moved along the time-coded trajectory from (e) initial to (f) final position; the used laser power is about 1mW. (g),(h) FCPM cross sections of a planar-aligned cholesteric cell with a layer dislocation without (g) and with (h) a graphene flake entrapped in the dislocation. The equilibrium cholesteric pitch is about 5 μm. The color-coded time scales in the insets of (b,e) show the elapsed time in seconds. The helical axis **χ**, crossed polarizer (P), analyzer (A), and coordinate axes are marked using red arrows.

#179756 - $15.00 USD Received 12 Nov 2012; revised 24 Dec 2012; accepted 24 Dec 2012; published 11 Jan 2013

Table 1. Material parameters of the used nematic LCs.

	K_{11}, pN	K_{22}, pN	K_{33}, pN	K, pN	n_o	n_e
5CB	6.4	3	10	≈7	1.536	1.714
ZLI-2806	14.9	7.9	15.4	≈11	1.475	1.518

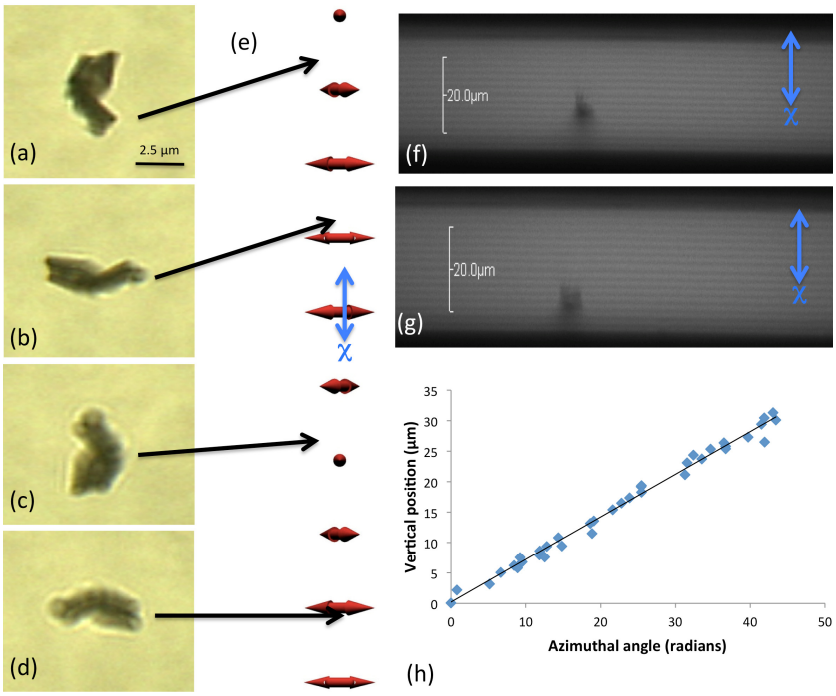

Fig. 2. Vertical translation of a graphene flake across a cholesteric layered structure. (a),(b),(c),(d) Optical micrographs showing an ascending graphene flake suspended in a cholesteric LC when pushed by a defocused laser trap of power ~1 mW, with the focus originally located about 10 μm above the flake. (e) A schematic representation of **n**(**r**) in a cholesteric structure, with the black arrows indicating flake positions along the helical axis **χ** shown by the blue double arrow (perpendicular to cell substrates and rotating **n** shown by red double arrows). (f),(g) FCPM imaging of the ascent of a graphene flake through the cholesteric layered structure, showing the starting (f) and ending (g) vertical positions of the flake. (h) Vertical position of a graphene flake in a cholesteric with p = 5 μm vs. the azimuthal orientation angle as the flake is moved via rotation and corresponding translation across a 30 μm cell using a laser trap of power ~1mW.

The well-efined azimuthal alignment of LC molecules with respect to crystallographic axes of graphene [21] results also in azimuthal surface anchoring of **n**(**r**) at the graphene-LC interface. The studied flakes are polydomain in nature and often have multiple folds [Fig. 1(a)], which cause **n**(**r**)-distortions around the flakes even when they equilibrate in the minimum-energy orientation. Such flake-induced distortions are clearly visible in PM textures obtained for a vertically aligned flake in a homeotropic nematic LC cell [Fig. 3(a)]. Alignment of **n**(**r**) caused by the polydomain structure of large-area graphene films has been observed before and was used to visualize the grain boundaries between these domains [21]. The competition of LC molecular alignment directions imposed by differently oriented domains (except for rare cases of single-domain flakes) results in a certain orientation of flake edges with respect to $\mathbf{n_0}$ (while typically keeping the flake faces parallel to $\mathbf{n_0}$) and this orientation typically undergoes weak fluctuations (up to 2-5 degrees, depending on lateral size). The ensuing **n**(**r**)-distortions are important from the standpoint of view of optical manipulation discussed below.

#179756 - $15.00 USD Received 12 Nov 2012; revised 24 Dec 2012; accepted 24 Dec 2012; published 11 Jan 2013

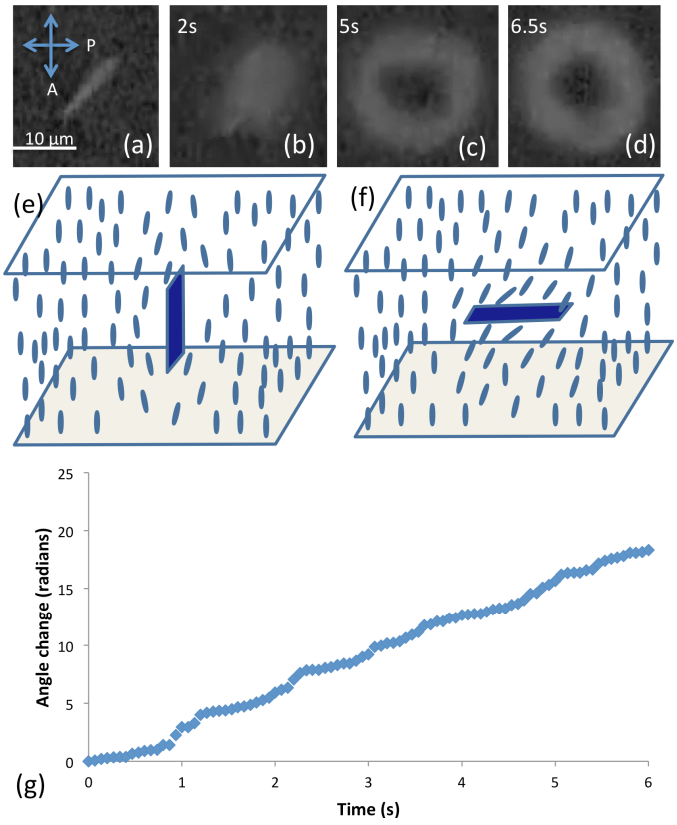

Fig. 3. Laser-induced spinning of a flake in a nematic LC. (a) Optical PM image of a vertically aligned graphene flake in a 20 µm homeotropic nematic cell. (b),(c),(d) Optical PM micrographs showing realignment and rotation of a graphene flake in a laser trap. When the trap is turned on, a vertically aligned flake (b) flips sideways and spins (c-d). The optical images obtained between crossed polarizers highlight the local distortions in the nematic director caused by the spinning graphene flake. The elapsed time is marked on images. (e) A schematic representation of a graphene flake aligned vertically in a homeotropic cell corresponding to the image shown in (a). (f) A schematic representation of a spinning graphene flake and director distortions corresponding to images (c-d); the arrow indicates the spinning direction around the axis normal to the cell substrates. (g) Azimuthal orientation angle of the flake vs. time corresponding to images shown in (c) and (d).

3.2 Non-contact optical manipulation of flakes in nematic and cholesteric liquid crystals

Optical trapping and manipulation of graphene flakes in isotropic fluid hosts, such as water, previously revealed that the interplay between optical and shape anisotropy of these flakes is crucial in determining the alignment and diffusion of graphene in an optical trap [20]. In particular, it was shown that optically trapped submicrometer graphene flakes suspended in water tend to align with the plane of the flake parallel to the light propagation direction and perpendicular to the linear polarization direction [20]. This behavior is in contrast to that of optically trapped transparent platelets and other anisotropic particles that tend to align parallel to the light propagation direction and polarization [6,16]. In LC hosts, however, the trapping behavior is very different as the surface anchoring tends to align the flakes parallel to $\mathbf{n_0}$ and both LC and graphene refractive indices are polarization-dependent. The complex refractive index of graphene in the near infrared part of spectrum is $n_{g\perp} \approx 3 + 1.5i$ for light linearly polarized perpendicular to the graphene's C-axis (parallel to the flake) and $n_{g||} \approx 1.694$ for polarization parallel to the C-axis [20–23]. Both ordinary and extraordinary LC refractive indices are higher than that of water used as a host medium in the previous studies [20] and

#179756 - $15.00 USD Received 12 Nov 2012; revised 24 Dec 2012; accepted 24 Dec 2012; published 11 Jan 2013

comparable to $n_{g||}$ but much smaller than the real part of $n_{g\perp}$ (Table 1). Additionally, the laser-trapped graphene is accompanied by the anchoring-induced LC polydomain distortions that span to micrometer-range distances, much larger than the flake thickness, so that trapping of flakes cannot be described without considering these distortions, as discussed below in detail.

In our experiments, the balance of optical gradient, scattering, surface anchoring, and elastic forces results in laser trapping with flakes perpendicular to the trapping beam axis and typically parallel to $\mathbf{n_0}$. Optical absorption of trapped graphene flakes (highly dependent on their orientation) is relatively small for their orientation perpendicular to the beam, but still can result in photothermal heating of the flakes and the surrounding LC. To mitigate this problem while manipulating graphene in the LC mesophases, we have used relatively low laser powers < 5 mW at which no melting of LC to an isotropic state is observed and laser-induced heating effects can be neglected. Tight focusing of a laser beam at these laser powers enables robust three-dimensional (3D) optical manipulation of graphene flakes in LCs (Figs. 1 and 2), similar to that previously demonstrated in isotropic fluid hosts [20]. For example, in a planar-aligned cholesteric LC, the flakes are optically translated along computer-guided trajectories within both a uniform helical structure [Fig. 1(b), 1(c)] and also along an edge dislocation [Fig. 1(d)-1(h)].

Unlike in isotropic solvents [20], 3D optical manipulation of flakes in LCs is primarily due to the director distortions around flakes (caused by the folding and polydomain nature), which are significantly thicker than the flakes themselves. Since the local effective refractive index in the vicinity of a flake is highly dependent on $\mathbf{n}(\mathbf{r})$ with respect to the light propagation and polarization directions, one can select the linear polarization direction of the trapping laser beam for which flake-induced distortions of $\mathbf{n}(\mathbf{r})$ have refractive index higher than that of the surrounding LC. The maximum achievable contrast of the effective refractive index between the LC regions in the vicinity of a flake and far away from it is limited by the values of optical anisotropy, which is 0.2 for 5CB and 0.04 for ZLI-2806 (Table 1). The presence of the high-index graphene flake further enhances the refractive index contrast between the flake with induced $\mathbf{n}(\mathbf{r})$-distortions and the surrounding LC, thus enabling robust polarized-light 3D optical manipulation by means of a combination of gradient and scattering forces (Fig. 1).

One can estimate the strength of optical trapping forces using the balance of a peak value of trapping force (often called "trap escape force") with the viscous drag force. Since the system is highly overdamped (Reynolds number << 1), inertial forces are negligible and the trapping force F_t is balanced by a viscous Stokes drag $|\boldsymbol{F_t}| = |\boldsymbol{F_{drag}}| = \zeta V$, where ζ is a drag coefficient and V is velocity of particle translation [6,12]. To estimate ζ of a graphene flake in LC, we use an expression $\zeta = 16\eta D/3$ for the drag coefficient of a thin circular disk of diameter D that circumscribes the edges of a random-shaped flake [6]. For typical $\eta \approx 0.075$ Pa·s [6,24] and $D = 5$ μm, we find $\zeta \approx 2\text{x}10^{-6}$ kg/s. Although these estimates neglect the coupling of $\mathbf{n}(\mathbf{r})$ to the flow field, such simplified analysis is reasonable because the velocities of the flakes during the optical translation are small (≤ 2 μm/s). The estimates yield the peak value of achieved laser trapping force of $F_t \approx 4$ pN at laser powers up to 5 mW. Alternatively, the trapping force can be also estimated from its balance with the known defect line tension of the so-called Lehman cluster, which is ≈35 pN for a cholesteric LC with p ≈5μm composed of ZLI-2806 and CB-15 [24], when stretching it in the direction perpendicular to the defect line. We obtain comparable values of $F_t \approx 3$ pN; the slightly smaller value of the peak trapping force may be caused by the proximity of the Lehman cluster that alters the spatial distribution of the effective refractive index around the flake during the stretching experiment. Although the achieved optical trapping forces are relatively weak, mainly because of the necessity of using low laser trapping powers, they are sufficient for robust translational optical manipulation of graphene flakes in LCs (Figs. 1 and 2).

#179756 - $15.00 USD Received 12 Nov 2012; revised 24 Dec 2012; accepted 24 Dec 2012; published 11 Jan 2013

3.3 Vertical translation of flakes by scattering forces and measurement of cholesteric pitch

When the laser beam of our HOT setup is focused several micrometers behind a flake, we observe that the flake is pushed across the cell and along the light propagation direction by scattering forces (Fig. 2). If the LC is of cholesteric type with the helical axis normal to the cell substrates, this translation is coupled to rotation of flakes (Fig. 2) [15,16]. When pushed along the helical axis, a flake rotates and follows the helicoidal **n**(**r**), as clearly seen for a low-symmetry random-shaped flake shown in Fig. 2(a)-2(g). The vertical position of a flake is a linear function of the azimuthal angle of the in-plane flake orientation [Fig. 1(h)] which traces **n**(**r**) with $n_x = \cos(2\pi z/p)$, $n_y = \sin(2\pi z/p)$, and $n_z = 0$ (as deduced by means of video microscopy by tracking rotation of edges of asymmetric flakes). From the best linear fit of the experimental data, we obtain cholesteric pitch of 4.45 μm, which is close to the equilibrium pitch p = 5 μm prepared by mixing the nematic host and CB15 as described in section 2.1 above. This behavior of flakes resembles that of nanorods and nanowires dispersed in cholesteric LCs [15,16], which also enable measurements of the cholesteric pitch by utilizing similar experiments.

3.4 Flake-assisted realignment of LC director and flake spinning in a polarized laser trap

When a low-power trapping laser beam of about 1.2 mW or higher is focused into a diffraction-limited spot (of about 0.8 μm in diameter) on a vertically aligned graphene flake in a homeotropic LC cell, we observe that the flake first rotates to the in-plane orientation parallel to glass plates and then starts spinning. Using PM and gradually increasing power of a focused laser beam in the graphene-free area of the same cell, the conventional optical Freedericksz transition threshold power was experimentally determined to be much higher (about 70 mW in a cell of thickness d = 20 μm) and consistent with the known expression for threshold intensity in a homeotropic nematic cell [16] $I_{th} = \pi^2 K_{33}\, n_e^2 c / [(n_e^2 - n_o^2)\, n_o\, d^2]$, where K_{33} is a Frank elastic constant for bend deformations, n_e and n_o are the extraordinary and ordinary refractive indices at the beam's wavelength, respectively (Table 1), and c is the speed of light. The flake (initially parallel to the linear laser polarization direction) and its pre-existing director distortions mediate rotation of the flake and **n** in the cell midplane at much lower powers ≥0.6 mW. Interestingly, optical trapping and the laser-induced realignment of flakes by the laser trap has been observed previously in isotropic solvents at comparable laser powers of about 1 mW [20]. In an LC medium, one can expect that the LC elasticity tends to resist rotation of the flake away from its initial orientation parallel to the far-field director $\mathbf{n_0}$; it is therefore likely that this reorientation is also assisted by the pre-existing director distortions around the flakes that result in further augmenting of the optical torque acting on the flake itself. Consistent with this hypothesis, the laser powers needed for reorienting different flakes vary in the range 0.5-5 mW, indicating that the polydomain nature of flakes and distortions around them (unique for each flake) may play an important role in this effect.

Although spinning of birefringent particles in isotropic and LC media due to optical angular momentum transfer from a trapping beam to the particle was reported before [24], an unexpected observation is that the graphene flake spins even when trapped by a linearly polarized Gaussian laser beam (Fig. 3). We attribute this to the fact that the **n**(**r**)-distortions above and below the flake change laser polarization from linear to circular (or elliptical) as light traverses through the LC. This is consistent with the observed time-varying rotation rate at a constant power [Fig. 3(g)], which is likely caused by continuous changes of elliptical polarization state of the trapping beam as the flake rotates and the flake-induced **n**(**r**)-distortions around it change. Because of vertical boundary conditions and homeotropic alignment far away from a spinning flake in the laser trap, LC elasticity does not favor any specific in-plane alignment of the flake, and thus spinning can be achieved at low laser powers of about 1mW via optical angular momentum transfer [24,25]. Since the **n**(**r**)-

#179756 - $15.00 USD Received 12 Nov 2012; revised 24 Dec 2012; accepted 24 Dec 2012; published 11 Jan 2013

structure across the sample thickness and thus also the beam's polarization in the focal plane change as the flake rotates, the transferred optical angular momentum and the rotation rate vary with time [Fig. 3(g)].

3.5 Laser-induced spinning of trapped flakes in a cholesteric LC

The vertical translation of graphene flakes by scattering forces due to a defocused laser beam (Fig. 2) shows that they tend to adopt a well-defined orientation with respect to both the helical axis $\boldsymbol{\chi}$ and $\mathbf{n}(\mathbf{r})$ in a planar-aligned cholesteric LC. However, we also find that a trapped graphene flake can spin in both linearly and circularly polarized laser traps (Fig. 4), with the spinning rates being typically at maximum for circularly polarized trapping laser beams and dependent on the flake location in a sample. The spinning rates are constant in time [Fig. 4(a)], linearly increase with the laser power [Fig. 4(b)], and are determined by the competition between the optical and viscoelastic torques exerted on a flake and $\mathbf{n}(\mathbf{r})$-distortions around it. Interestingly, the flakes with folds often adopt somewhat different orientations with respect to $\boldsymbol{\chi}$ and the trapping beam's axis. These different orientations result in different spinning rates, with the orientation of flakes confined into a plane perpendicular to $\boldsymbol{\chi}$ corresponding to the highest spinning rate [Fig. 4(b)]; this result is natural as elastic and viscous forces that resist such spinning are at minimum in this case.

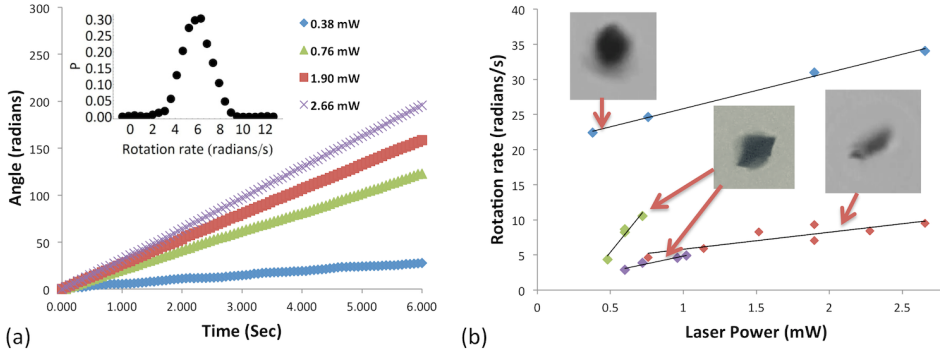

Fig. 4. Laser-induced spinning of flakes in a cholesteric LC. (a) Azimuthal orientation angle of a flake vs. time for different laser trap powers. The inset shows a normalized probability distribution P of measured rotation rates at the laser trap power of W = 2.4 mW. (b) Rotation rate vs. laser power for different graphene flakes and trap polarizations. The blue and red diamonds show experimental rotation rates vs. laser power for linearly polarized trapping beam and for the same flake but when it is folded and oriented differently with respect to the beam axis (shown in the insets). The purple and green diamonds show rotation rates for a flake trapped by a laser beam with linear (purple) and circular (green) polarizations. Best linear fits of experimental data are shown by solid black lines.

The optical torque applied to a graphene flake surrounded by $\mathbf{n}(\mathbf{r})$-distortions is $\tau_o = \Delta\sigma W/\omega$, where $\Delta\sigma$ is the change in the degree of circular polarization as the beam passes through the LC cell with flake and director distortions around it, W is the laser power, $\omega = 2\pi c/\lambda$ is the optical angular frequency, and λ is the wavelength [25]. The polarization state changes as the trapping light traverses through the LC above and below the flake. Regardless of the polarization state of the incident laser light, the polarization of the beam at the plane of the flake is generally elliptical in both nematic and cholesteric LCs (Figs. 3 and 4). Therefore, spinning of a flake can be achieved by using laser-trapping beams with both circular and linear initial polarization states (Figs. 3 and 4), as also observed in the case of spinning cholesteric LC droplets [26]. Since the viscous drag torque τ_v applied to the rotating flake is proportional to its angular rotation frequency Ω, the linear dependence of Ω vs. W (Fig. 4) is consistent with this model. Future studies will need to explore the effects of flake-induced heating at high laser powers and the role of elastic coupling between a flake and $\mathbf{n}(\mathbf{r})$ as the

#179756 - $15.00 USD Received 12 Nov 2012; revised 24 Dec 2012; accepted 24 Dec 2012; published 11 Jan 2013

flakes spin in the laser trap. Since anisotropic nanoparticle spinning effects in linearly polarized trapping laser beams have been also reported for several different types of particles dispersed in isotropic solvents such as water [27–30], it will be of interest to explore how the interplay of anisotropy of a particle (with controlled geometric shapes defined by means of, say, photolithography [31]) and the surrounding medium can be utilized to make these effects even more robust and better controlled, as needed for applications in light-driven micro-machines. A comparative analysis of trapping and spinning behavior of graphene and other anisotropic particles in both isotropic and anisotropic solvents may also provide deeper insights into the physical underpinnings of these phenomena.

4. Conclusion

We have demonstrated translational and rotational non-contact optical manipulation of dispersed self-aligned graphene flakes in both nematic and cholesteric liquid crystals as well as graphene-enhanced realignment of the LC director. Potential applications include optically- and electrically-controlled reconfigurable composites and devices based on ordered LC dispersions of spontaneously aligning colloidal graphene flakes [32]. Our findings may allow for bulk optical patterning of transparent conductive electrodes in the form of interconnected graphene flakes and further expand the applications of graphene in LC-based electro-optic devices and displays [33,34]. We have shown that graphene flakes allow for the realignment of the LC director at threshold laser powers much lower than in graphene-free LCs under otherwise similar conditions. An interesting observation is also the transfer of optical angular momentum from trapping laser beams to flakes in various types of LCs that may be utilized for microrheological studies of these soft matter systems [35].

Acknowledgments

We acknowledge the support of the Institute for Complex Adaptive Matter (ICAM) and the NSF grants DMR-0844115 (C.W.T. and I.I.S.) and DMR-0847782 (J.S.E and I.I.S.). We thank T. Lee, A. Martinez, B. I. Senyuk, and R. P. Trivedi for technical assistance with different aspects of this work. We also acknowledge discussions with N. A. Clark and R. P. Trivedi.

#179756 - $15.00 USD Received 12 Nov 2012; revised 24 Dec 2012; accepted 24 Dec 2012; published 11 Jan 2013